Studies of spherical tori, stellarators and anisotropic pressure with the M3D code

L.E. Sugiyama[a], W. Park[b], H.R. Strauss[c], S.R. Hudson[b], D. Stutman[d], X.-Z. Tang[b]

[a] Massachusetts Institute of Technology, Cambridge, Massachusetts
[b] Princeton Plasma Physics Laboratory, Princeton University, Princeton, New Jersey
[c] New York University, New York, N.Y.
[d] Johns Hopkins University, Baltimore, Maryland

United States of America

Abstract. The Multi-level 3D (M3D) project simulates plasmas using multiple levels of physics, geometry and grid models in one code package. The M3D code has been extended to fundamentally non-axisymmetric and small aspect ratio, $R/a \gtrsim 1$, configurations. Applications include the non-linear stability of the NSTX spherical torus and of the spherical pinch, as well as the relaxation of stellarator equilibria. The fluid level physics model has been extended to evolve the anisotropic pressures $p_{j\parallel}$ and $p_{j\perp}$ for the ion and electron species and has been applied to magnetic island evolution.

1. Introduction

The Multi-level 3D (M3D) project [1] carries out numerical simulation studies of plasmas using multiple levels of physics, geometry and grid models in one code package. The M3D code has been extended to fundamentally non-axisymmetric and small aspect ratio, $R/a \gtrsim 1$, configurations. Applications include the NSTX spherical torus, the spherical pinch and stellarators. The fluid level physics model has been extended to evolve the anisotropic pressures $p_{j\parallel}$ and $p_{j\perp}$ for ions and electrons, which includes the neoclassical collisional parallel viscous stresses.

2. The spherical torus

Discharges in NSTX [2] experience internal reconnection events (IREs), with substantial global energy loss, when the value of the safety factor q in the central core of the plasma is near 2 or near 1. To obtain insight into the mechanism of these events, cases with $R/a = 1.3$ and peak beta about 10% were studied using the M3D code.

When the core $q \simeq 2$ both experimental data and the M3D simulation indicate that a double tearing reconnection, associated with the existence of two $q = 2$ surfaces in the plasma, causes an IRE. The q profile is not measured directly. The experimental SXR data show that the core crash propagates inwards from off-axis. Simulations show that a double tearing reconnection can occur when two $q = 2$ surfaces exist. It further suggests that a single $q = 2$ surface tends to be stable.

The first case in Fig. 1 shows simulation results for a double tearing reconnection. Temperature contours in two plasma cross-sections are shown in Fig. 1(a), where the growing inner $m = 2$ islands encroach on the core region. The simulated 'SXR' lines of sight and simulated 'ECE' origination locations on the midplane are also shown. Figure 1(b) shows the calculated SXR signals in time and Fig. 1(c) the electron temperature derived from the calculated ECE signals, presented as contours in the (minor radius, time) plane. At present, it is difficult to compare the SXR signals between experiment and theory because the experiment (so far) has been ohmic and the plasma rotation is slow. More importantly, the theoretical SXR signals for this type of instability show no strong distinguishing features (Fig. 1(b), compare with the $q \simeq 1$ case in Section 3). The temperature contour plot from the ECE (Fig. 1(c)), on the other hand, maps the topological changes clearly. One can see, for example, the core region being completely reconnected with the inner $m = 2$ islands. Although ECE detection is not feasible in NSTX, due to the low field cut-off, the planned electron Bernstein wave (EBW) measurement of temperature should allow a detailed comparison with theory.

Simulation results for an IRE with $q \simeq 1$ are shown in Figs 1(d)–(f). The SXR signals show a classic sawtooth precursor and crash, Fig. 1(e), as does experiment (not shown). Experimental data further

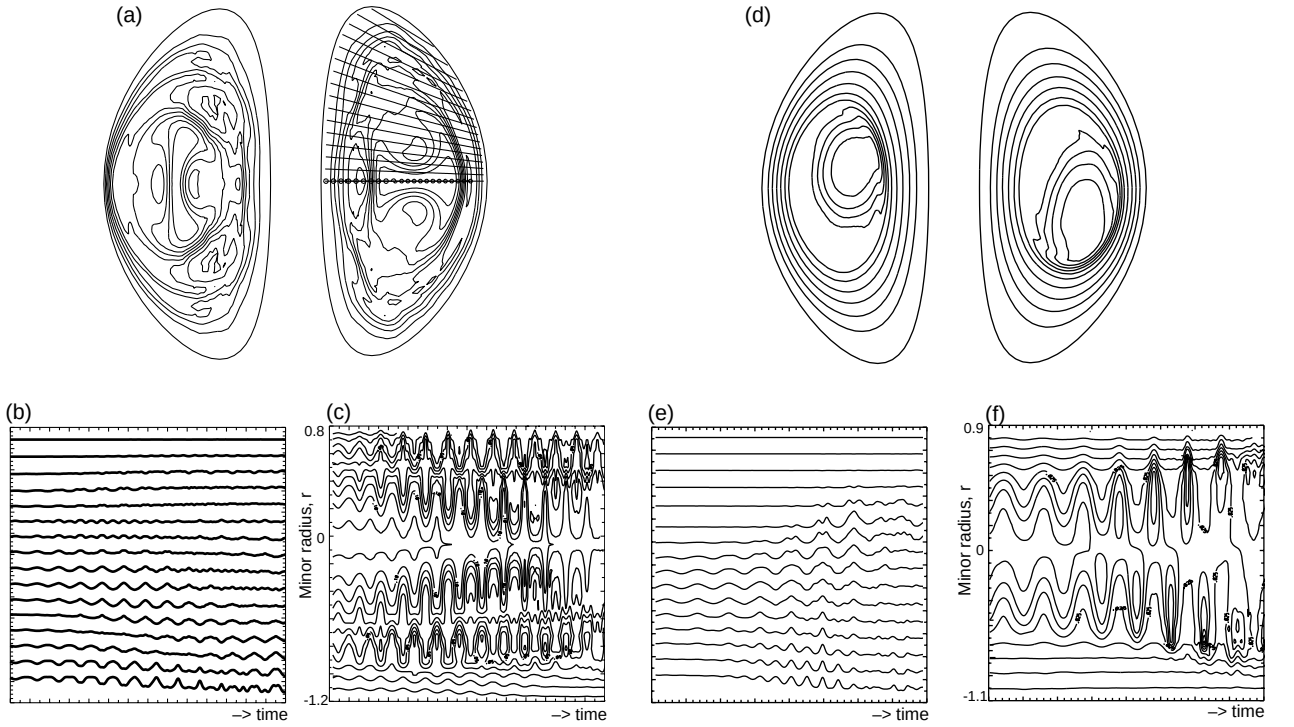

Figure 1. Simulation of two types of IREs in NSTX. Double tearing reconnection with core $q \simeq 2$ and two $q = 2$ surfaces: (a) temperature contours at two cross-sections, $\phi = \pi$ and $\phi = 0$, also showing lines of sight for the simulated SXRs and midplane positions for the ECE signals; (b) time plot of SXR signals, (c) ECE signals, shown as T_e contours in the (r, t) plane. Case with core $q \simeq 1$: (d) temperature contours, (e) time plot of SXR signals; (f) ECE signals, shown as T_e contours in the (r, t) plane.

show that the plasma rotation slows before the final crash, possibly locking to the resistive wall. There are also indications that a localized medium n (toroidal mode number) instability may sometimes develop just before the final crash. This could be driven by the local pressure bulge produced by the initial low n modes, as in high β tokamak disruptions [3]. These questions are being further investigated in experiment and simulation.

3. Spherical pinches

Spherical pinches (SPs) are promising low aspect ratio toroidal devices with a reversed shear rotational transform, which combine features of the spherical torus and the pinch. Toroidal pinches have poloidal and toroidal components of the magnetic field of comparable magnitude, $qR/a \approx 1$. They tend to have reversed magnetic shear, which can be favourable for confinement. Reversed field pinches typically have $R/a \simeq 5$, $q \simeq 0.2$. Their confinement is poor due to MHD activity, because of the many resonances with poloidal mode number $m = 1$. SPs have $R/a \simeq 1$ and $q \simeq 1$ and can be tailored to have q profiles satisfying $1 > q > \hat{m}/(\hat{m} + 1)$. Taking $\hat{m} \geq 1$ then eliminates the $m = 1$ resonances and allows relatively high values of the plasma beta, similar to those of spherical tori. These special SPs have a monotonically decreasing q profile. The toroidal field is small at the outer edge, but does not reverse. Unlike a spheromak, there is an applied toroidal magnetic field.

Ideal MHD simulations of a typical SP with $R/a = 1.5$ were done with M3D, using a poloidal unstructured mesh [4, 5] of 2500 points and a spectral representation in the toroidal angle. The plasma was assumed to have a rigid conducting wall boundary. Typical equilibrium profiles are shown in Fig. 2.

SP stability is determined by 'reverse ballooning' modes. Below an average $\langle\beta\rangle$ threshold, SPs are MHD stable ($\langle\beta\rangle \equiv 2\langle p\rangle/\langle B^2\rangle$, where the bracket is an average over the poloidal plane). Reverse ballooning resembles conventional low mode number ballooning, but the modes have maximum amplitude

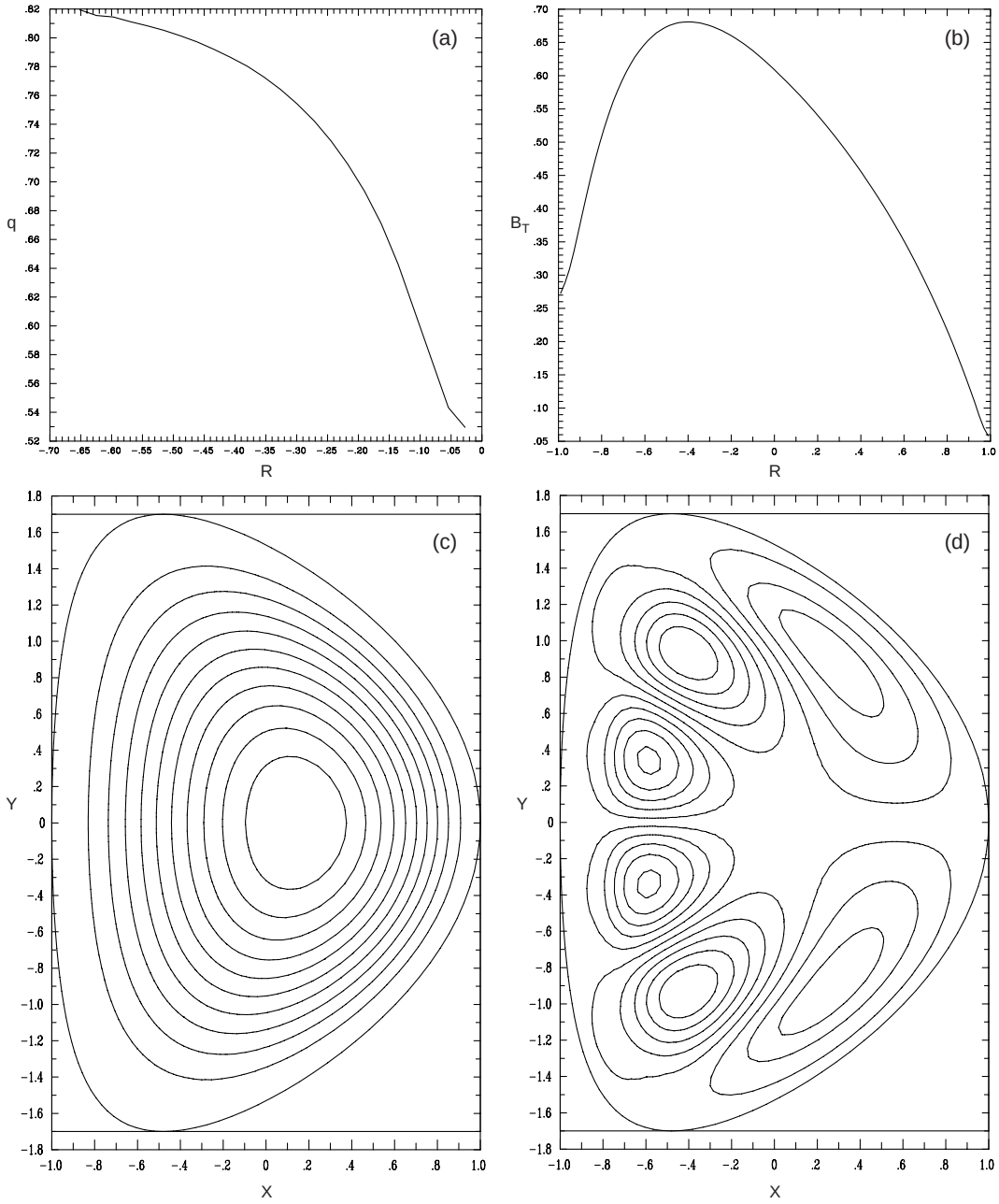

Figure 2. SP equilibrium profiles of (a) q and (b) toroidal magnetic field B_T as functions of R. (c) Pressure contours for $p \sim \psi$ and $\langle\beta\rangle = 12\%$. (d) Velocity potential of the unstable (3,4) linear mode in the poloidal plane $\phi = 0$.

on the inboard, high field side, apparently due to the reversed shear and low aspect ratio.

In the example, modes associated with the lowest resonances, $(m, n) = (2, 3)$ and $(3, 4)$, are unstable (Figs 2(d) and 3).

The value of the critical $\langle\beta\rangle$ depends on the shape of the equilibrium pressure profile. Figure 3 compares the ideal MHD growth rates for two different pressure profiles, $p \sim \psi$ and $p \sim \psi^{3/2}$, for two toroidal mode numbers, $n = 3$ and 4. The broader profile, $p \sim \psi$, is more stable, with a critical $\langle\beta\rangle \simeq 15\%$. Yet broader profiles may have higher $\langle\beta\rangle$. (In the plot, the marginal stability points were interpolated after finding stable damped modes.)

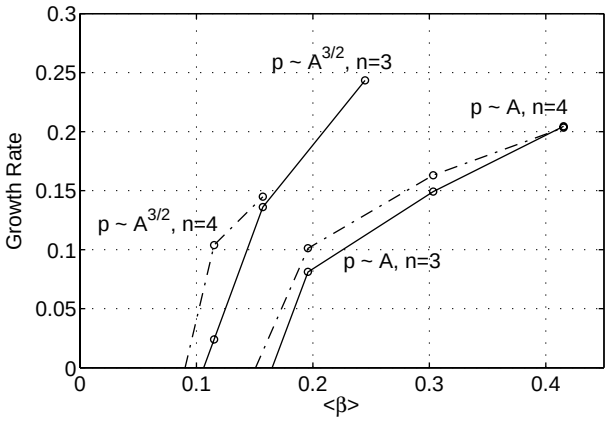

Figure 3. Ideal MHD growth rate versus $\langle\beta\rangle$ for the $n = 3$ and 4 modes, for SP equilibria with $p \sim \psi$ and $\psi^{3/2}$.

An unstable high β SP with reversed shear disrupts non-linearly by distortion of the high field side. The lowest mode numbers appear to dominate the evolution, as shown by the pressure contours in Fig. 4.

4. Stellarators

To model stellarators and other fundamentally non-axisymmetric configurations, M3D uses a mesh with a three dimensional spatial variation. For a stellarator, output from the VMEC equilibrium code [6] can be used to construct an initial M3D equilibrium. This initial state is then relaxed under the influence of resistive dissipation, cross-field thermal conduction and parallel thermal conduction (simulated with the 'artificial sound' method [7, 13]), while using source terms to maintain the desired toroidal current and pressure. The kinetic energy is removed by viscous damping. Equilibria have been obtained for LHD [8], W7-X [9], and the proposed compact quasi-axisymmetric (QAS) stellarator [10]. Detailed comparison with the PIES code [11] is in progress.

Simulations of the QAS used a mesh of 6000 poloidal points with 36 toroidal planes. Figure 5 shows the relaxation of QAS equilibrium li383 at the design pressure. Although VMEC assumes perfect flux surfaces, its output current lacks the singularities needed to prevent island formation at rational surfaces. When this current is used to calculate the

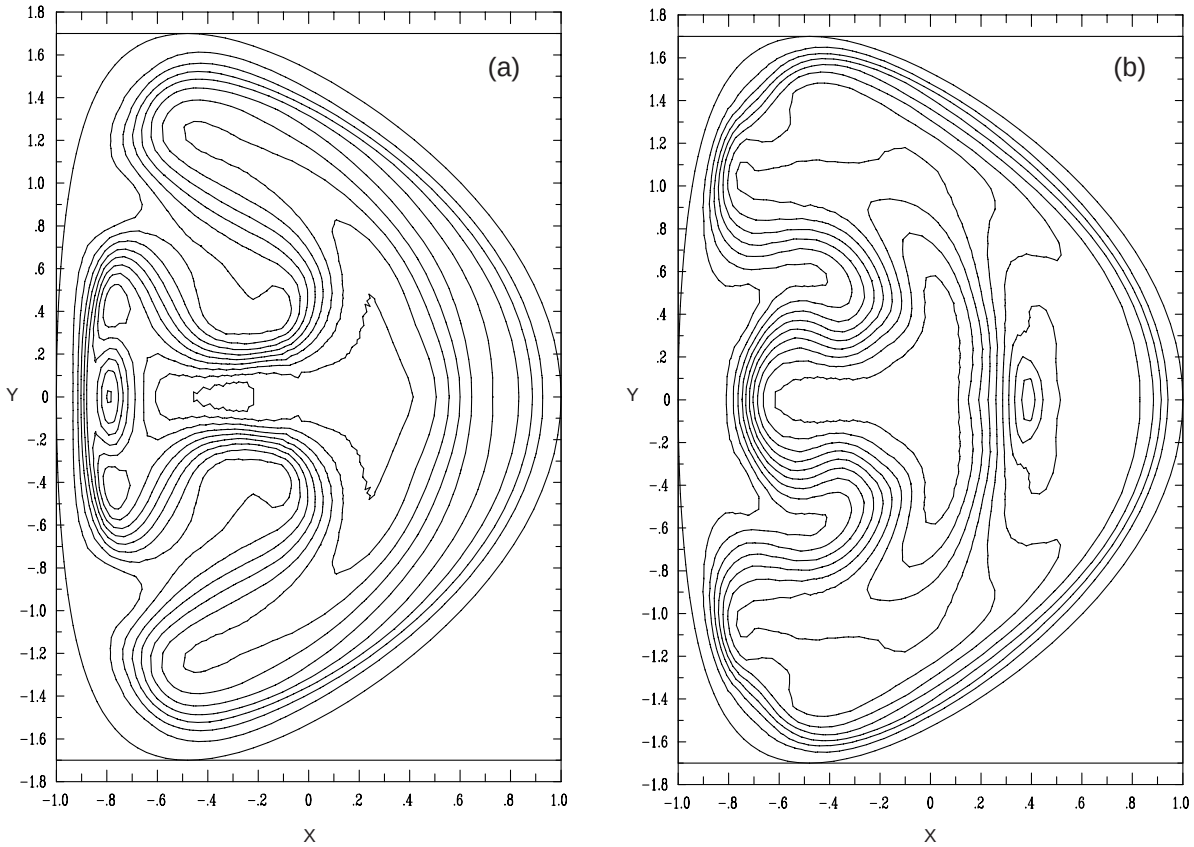

Figure 4. Non-linear 'reverse ballooning' pressure contours at $t = 37\tau_A$ for (a) $\phi = 0$ and (b) $\phi = \pi$.

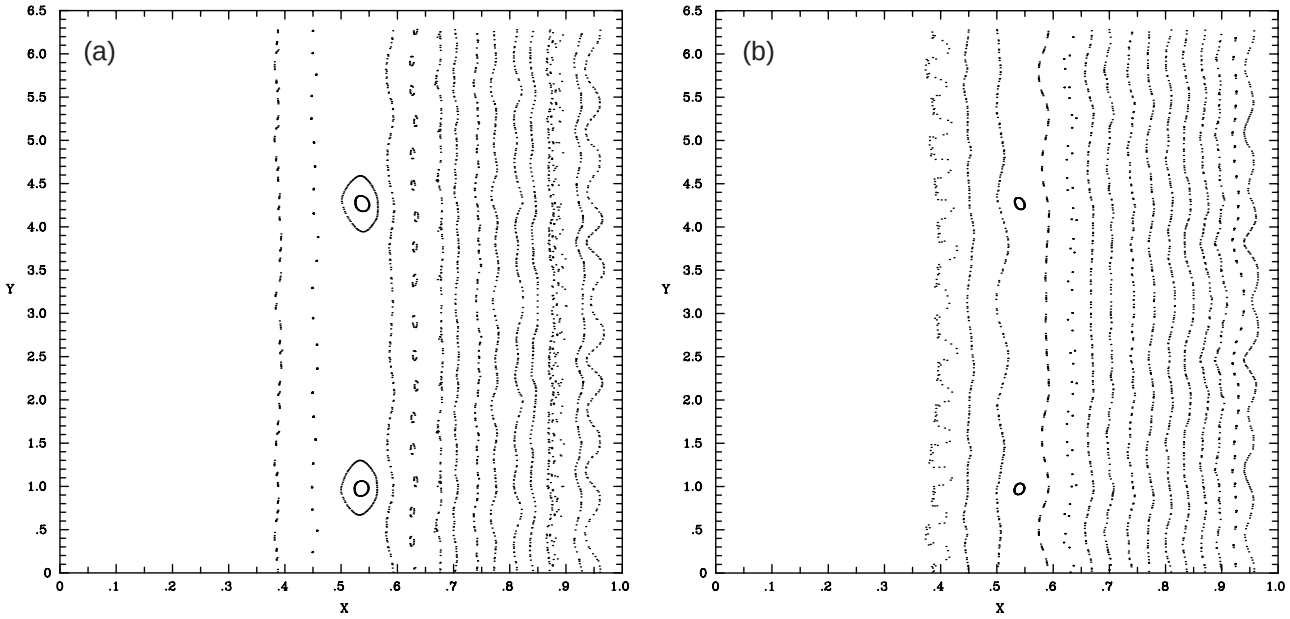

Figure 5. Field line plots showing the relaxation of QAS equilibrium li383 from (a) an initial VMEC equilibrium at $t = 0$ and (b) a relaxed state at $t = 20\tau_A$.

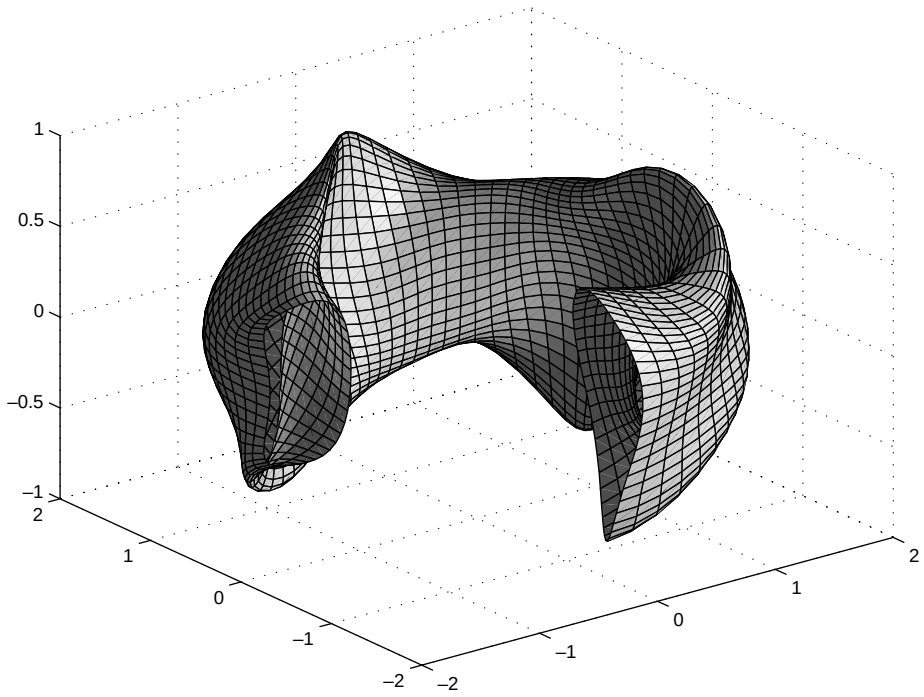

Figure 6. Relaxed QAS equilibrium li383.

initial magnetic field in M3D, the configuration contains islands (Fig. 5(a)). The islands tend to shrink during relaxation (Fig. 5(b)). Figure 6 shows the relaxed equilibrium configuration. At high enough pressure, however, the plasma becomes unstable to ballooning modes (Fig. 7).

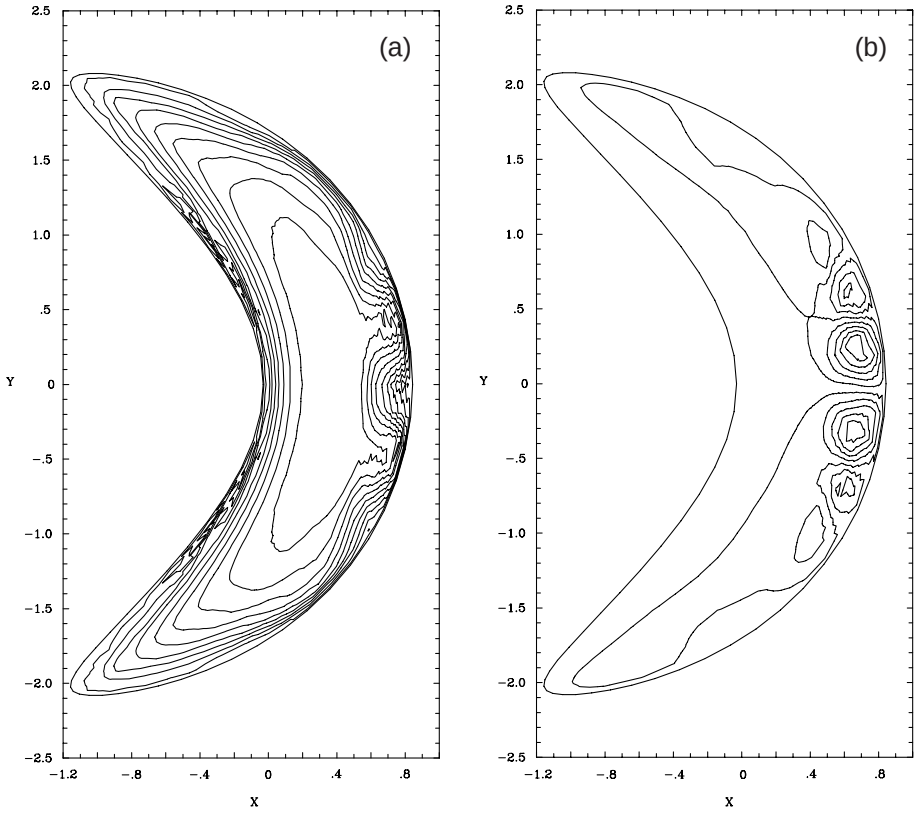

Figure 7. At twice the design pressure, the configuration is ballooning unstable, as shown by the contours of (a) pressure and (b) velocity potential at $t = 32\tau_A$.

5. Anisotropic fluid pressure

To improve the fluid (MHD/two fluid/neoclassical) description of a confined plasma, the anisotropic pressure components $p_\parallel$ and $p_\perp$ can be evolved and the moments closed using the heat fluxes $q_\parallel$ and $q_\perp$. M3D now evolves the anisotropic temperatures $T_{j\parallel}$ and $T_{j\perp}$ for electrons and ions j, through equations for the average temperatures $T_j = (T_{j\parallel} + 2T_{j\perp})/3$ and the anisotropies $\delta T_j = T_{j\parallel} - T_{j\perp}$, using a collisional form of the δT equations with relatively simple expressions for the collision terms (similar to those of Ref. [12]). The density (continuity) equation is solved separately. The M3D heat fluxes include the effects of parallel and cross-field thermal conduction, the parallel part modelled as thermal equilibration along magnetic field lines ('artificial sound').

The collisional parallel viscous forces $\boldsymbol{\nabla} \cdot \boldsymbol{\Pi}_\parallel$, $\boldsymbol{\Pi}_\parallel = \delta p(-\boldsymbol{I}/3 + \hat{\boldsymbol{b}}\hat{\boldsymbol{b}})$, where $\delta p = n\delta T$, appear naturally, including the neoclassical enhancement to the polarization drift. Studies with M3D have shown [13] that in a torus the dominant role is played by the flux surface average of the viscous forces, rather than by (simple forms of) the poloidal variation, for the bootstrap current and other effects on the equilibrium and on the neoclassical tearing mode (NTM) [14, 15].

Simulations show that the non-linear growth/shrinkage of magnetic islands and its correlation with terms in the parallel Ohm's law is not simple. In NTM theory [14, 15] the pressure gradient flattens over a finite size island and the additional, flux surface averaged bootstrap current ($\propto \langle dp/d\psi \rangle$) drives island growth (Figs 8(a) and (b)). The collisional viscous force calculated from evolving δT is more variable (Fig. 8(c)) and its flux surface average (taken with respect to the equilibrium field) tends to overshoot to positive values inside a growing island (Fig. 8(d)), rather than tending to zero. In both cases, the magnetic axis and edge values are zero.

The neoclassical pressure anisotropy in $\boldsymbol{\nabla} \cdot \boldsymbol{\Pi}_\parallel$ becomes significant only at relatively high β and low resistivity. For the (2,1) resistive NTM, M3D results show that the related two fluid term $(1/en)\nabla_\parallel p_e$ in Ohm's law may also non-linearly destabilize magnetic islands, at lower β. It has no effect on the linear

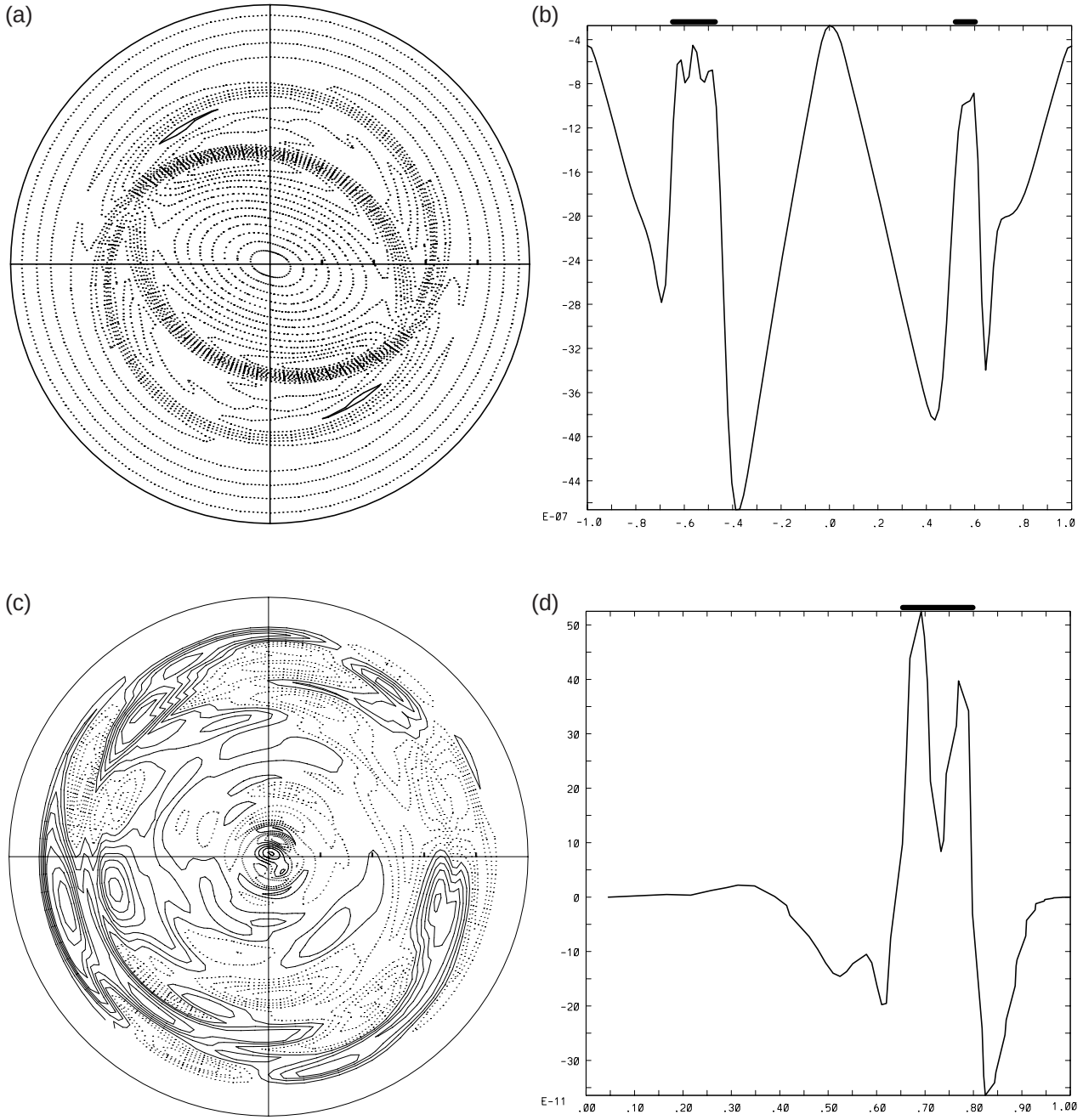

Figure 8. Parallel component of the electron collisional parallel viscous force $[1/(enB^2)]\boldsymbol{B}\cdot\boldsymbol{\nabla}\cdot\boldsymbol{\Pi}_{e\|}$ for large (2,1) islands, calculated using the flux surface averaged neoclassical expressions for ions and electrons $(1/nm_j)(nm_j/\tau_j)\mu_{0j}U_{\theta j}$, where μ_{0j} is the neoclassical coefficient for the flow $U_{\theta j}$, with equilibrium $\nabla T_j = 0$ [13]. First case, (a) contours and (b) profile as a function of minor radius, left side along $\theta = \pi/2$ in (a) (upper vertical axis) and right side along $\theta = 0$ (right horizontal axis). Second case, calculated by evolving δT_j with $\nabla T_j \neq 0$, (c) contours and (d) flux surface average, based on the equilibrium field, as a function of minor radius $[0, a]$. Axis and edge values are zero. The bars at the top show the location of islands.

mode. Although typically $\boldsymbol{B}\cdot\boldsymbol{\nabla}T_e \simeq 0$, $\boldsymbol{B}\cdot\boldsymbol{\nabla}p_e$ can be significant if the density is allowed to evolve. In equilibrium, $(\delta n)_\|/n \sim O(\delta p/p)$. Non-linearly, the density equilibrates along field lines due to the effects of sound waves acting on the pressures and perpendicular thermal conduction, which is slow

compared with the electron temperature equilibration. This was confirmed for the (2,1) island by applying an accelerated parallel equilibration to p_e at fixed density, rather than to T_e, in the case when the entire gradient $\boldsymbol{\nabla} p_e$ was kept in Ohm's law. The island then behaved like the ordinary resistive MHD case, without the fast growth due to the ∇p_e variation along the field lines. Adding the rest of the two fluid terms did not greatly change the non-linear rate of growth compared with just $\nabla_\parallel p_e$.

The non-linear non-MHD terms can also introduce significant $(2m, 2n)$ components. Certain terms, including the Ohm's law $\nabla_\parallel p_e$ and $\boldsymbol{\nabla} \cdot \boldsymbol{\Pi}_{e\parallel}$, drive island rotation. Resistive MHD islands tend to remain (2,1), but the other effects can lead to development of a (4,2) structure inside the original outer (2,1) structure. The (4,2) magnetic field lines are disjoint, i.e. each pair of opposite O points shares field lines within, but not between, pairs. Other effects also exist.

6. Summary

The M3D code has been extended to non-axisymmetric and small aspect ratio configurations. The fluid level physics model has been extended to include the pressure anisotropies $\delta p = p_\parallel - p_\perp$ for electrons and ions. Applications have been presented for the spherical torus (non-linear internal reconnection events in NSTX), the spherical pinch (MHD equilibrium and stability) and the low aspect ratio stellarator (relaxation of equilibria in QAS and comparison to the results of a stellarator equilibrium code). In a tokamak configuration, resistive magnetic islands have been found to grow non-linearly by mechanisms in addition to the neoclassical collisional parallel viscous force.

Acknowledgements

This work was supported in part by the US Department of Energy.

References

[1] Park, W., et al., Phys. Plasmas **6** (1999) 1796.
[2] Ono, M., et al., in Fusion Energy 1998 (Proc. 17th Int. Conf. Yokohama, 1998), Vol. 3, CD-ROM, IAEA, Vienna (2000) paper ICP/01, http://www.iaea.org/programmes/ripc/physics/start.htm.
[3] Park, W., et al., Phys. Rev. Lett. **75** (1995) 1763.
[4] Strauss, H.R., Longcope, D.W., J. Comput. Phys. **147** (1998) 318.
[5] Strauss, H.R., Park, W., Phys. Plasmas **5** (1998) 2676.
[6] Hirshman, S.P., Whitson, J.C., Phys. Fluids **26** (1983) 3553.
[7] Park, W., Monticello, D.A., Strauss, H., Manickam, J., Phys. Fluids **29** (1986) 1171.
[8] Iiyoshi, A., et al., Nucl. Fusion **39** (1999) 1245.
[9] Wagner, F., et al., in Fusion Energy 1998 (Proc. 17th Int. Conf. Yokohama, 1998), Vol. 1, CD-ROM, IAEA, Vienna (2000) paper OV2/4, http://www.iaea.org/programmes/ripc/physics/start.htm.
[10] Reiman, A., et al., ibid., paper ICP/06.
[11] Reiman, A.H., Greenside, H.S., J. Comput. Phys. **87** (1990) 349.
[12] Snyder, P.B., Hammett, G.H., Dorland, W., Phys. Plasmas **4** (1997) 3974.
[13] Sugiyama, L.E., Park, W., Phys. Plasmas **7** (2000) 4644.
[14] Carrera, R., et al., Phys. Fluids **29** (1986) 899.
[15] Qu, W.X., Callen, J.D., Plasma Rep. UWPR 85-5, Univ. of Wisconsin, Madison (1985).

(Manuscript received 5 October 2000
Final manuscript accepted 19 February 2001)

E-mail address of L.E. Sugiyama:
sugiyama@psfc.mit.edu

Subject classification: B0, Tt; B0, Te; B0, St; B0, Ct; C0, Tt; C0, Te; C0, St; C0, Ct